J. Fluid Mech. (2008), *vol.* 594, *pp.* 29–57. doi:10.1017/10.1017/S0022112007008737

Non-normality and nonlinearity in combustion–acoustic interaction in diffusion flames

KOUSHIK BALASUBRAMANIAN AND R. I. SUJITH†
Department of Aerospace Engineering, Indian Institute of Technology Madras, Chennai 600036, India

(Received 14 March 2007 and in revised form 29 July 2007)

The role of non-normality and nonlinearity in flame–acoustic interaction in a ducted diffusion flame is investigated in this paper. The infinite rate chemistry model is employed to study unsteady diffusion flames in a Burke–Schumann type geometry. It has been observed that even in this simplified case, the combustion response to perturbations of velocity is non-normal and nonlinear. This flame model is then coupled with a linear model of the duct acoustic field to study the temporal evolution of acoustic perturbations. The one-dimensional acoustic field is simulated in the time domain using the Galerkin technique, treating the fluctuating heat release from the combustion zone as a compact acoustic source. It is shown that the coupled combustion–acoustic system is non-normal and nonlinear. Further, calculations showed the occurrence of triggering; i.e. the thermoacoustic oscillations decay for some initial conditions whereas they grow for some other initial conditions. It is shown that triggering occurs because of the combined effect of non-normality and nonlinearity. For such a non-normal system, resonance or 'pseudoresonance' may occur at frequencies far from its natural frequencies. Non-normal systems can be studied using pseudospectra, as eigenvalues alone are not sufficient to predict the behaviour of the system. Further, both necessary and sufficient conditions for the stability of a thermoacoustic system are presented in this paper.

1. Introduction

The occurrence of combustion instabilities has been a plaguing problem in the development of combustors for rockets, jet engines and power-generating gas turbines (McManus, Poinsot & Candel 1993). Predicting and controlling combustion instability requires an understanding of the interactions between the combustion process and the acoustic waves. Combustion–acoustic interaction involves a feedback mechanism where the fluctuating heat release acts as a source of energy for the acoustic field and the latter in turn affects the combustion process and hence the heat release rate. A comprehensive prediction of the conditions for the onset of instabilities is a difficult task, which is not yet mastered. In particular, predicting the conditions under which finite-amplitude disturbances destabilize a linearly stable system and predicting the limit-cycle amplitude of the instability remain a key challenge, as little is known, even in a qualitative sense, about the key parameters controlling nonlinear flame dynamics, even in simple laminar flames (Zinn & Lieuwen 2005).

† Author to whom correspondence should be addressed: sujith@iitm.ac.in.

Combustion instability has been observed in both premixed and non-premixed combustors. A large number of investigations have been performed on combustion instability in premixed systems (see Lieuwen 2003 for a comprehensive review). As compared to premixed flames, not much work has been done on the combustion instability of non-premixed flames. However, most gas turbine combustors for aircraft and other industrial applications involve non-premixed combustion; therefore, it is important to investigate combustion instability in such systems.

There have been some studies regarding the unsteady nature of non-premixed flames. Hertzberg (1997) experimentally studied the effects of acoustic forcing on the flame shape and observed that at specific excitation frequencies and amplitudes, the driven flame splits into a central jet and side jets. Cuenot, Egoltopoulas & Poinsot (2000) investigated the effects of unsteadiness on counterflow diffusion flames using laminar flamelet models. They proposed an extinction diagram for the prediction of extinction conditions of unsteady counterflow flames, and it was found that there is a good agreement between the predicted and computed extinction points. Chaos *et al.* (2005) experimentally studied the effect of fuel Lewis number in unsteady Burke–Schumann hydrogen flames. Buckmaster, Jackson & Yao (1999), Jackson & Buckmaster (2000) and Buckmaster (2002) analysed the effect of unsteadiness on non-premixed flames in the context of propellant flame geometry and edge flames. These papers discuss the role of the Péclet number on the structure of the diffusion flame.

Vance, Miklavcic & Wichman (2001) studied the stability of a one-dimensional diffusion flame by analysing the effect of perturbations on the Burke–Schumann flame using linear stability analysis. Oscillatory and cellular flame instabilities were identified from the numerically calculated eigenvalues of the linearized system of equations. The role of convection in flame instabilities was also discussed. They also calculated (numerically) the critical values of various parameters affecting flame instability. Tyagi, Chakravarthy & Sujith (2007) investigated the unsteady combustion response of a ducted non-premixed flame and coupling with the duct acoustic field using numerical simulations. They considered a two-dimensional co-flowing non-premixed flame in a uniform flow field, as in the Burke–Schumann geometry. Both finite-rate and infinite-rate chemistry effects were examined. The one-dimensional acoustic field was simulated in the time domain using the Galerkin method, treating the fluctuating heat release from the combustion zone as a compact acoustic source. The combustion oscillations are shown to cause exchange of acoustic energy between the different natural modes of the duct over several cycles of acoustic oscillations. The authors emphasize the nonlinear nature of the interaction. However, the role of non-normality is not discussed.

The most complete solution to the problem can be obtained by solving the full compressible-flow equations. However, in many situations such as that encountered in the present paper, the combustion flow field is essentially incompressible (low Mach number) and solving compressible-flow equations to take account of the chamber acoustic field is computationally expensive and difficult. Alternatively, the combustion flow field can be solved using the incompressible-flow equations containing certain terms from the acoustic field, and the duct acoustic field can in turn be solved for, using linearized compressible-flow equations containing the source terms from the combustion flow field. This strategy was applied by Wu *et al.* (2003) for studying nonlinear premixed flame acoustic interaction. This approach was adopted by Tyagi *et al.* (2007) to study nonlinear effects in non-premixed flame acoustic interactions. The present paper adopts the same approach.

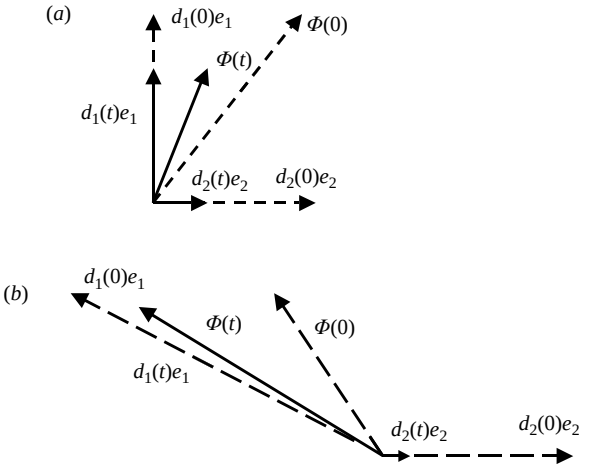

FIGURE 1. (*a*) Monotone decay of a normal system, (*b*) transient growth of a non-normal system. The initial state is $\Phi(0) = d_1(0)e_1 + d_2(0)e_2$, and the final state $\Phi(t) = d_1(t)e_1 + d_2(t)e_2$. The dashed lines denote the vectors at time $t = 0$ and the solid lines denote the vector at some time t.

The objective of this paper is to investigate the mechanism that leads to the complex interaction between the different eigenmodes of the coupled thermoacoustic system. We emphasize the role of non-normality in combustion–acoustic interaction. For such non-normal systems, linear stability analysis based on the analysis of individual eigenvalues is not sufficient to predict the behaviour of the system. Combustion–acoustic interaction is non-normal even when finite-rate chemistry effects are neglected.

Since there has been little work on combustion instability of non-premixed flames, the present approach is to retain only the most basic aspects of such a flame, to gain clear understanding. The configuration chosen is identical to that in Tyagi *et al.* (2007), i.e. a two-dimensional co-flow non-premixed flame in the Burke–Schumann geometry. Combustion is modelled using an infinite-rate chemistry model, where the flame is assumed to be a thin sheet. The roles of non-normality and nonlinearity are clarified in combustion–acoustic interactions in the context of such a diffusion flame. This paper is a continuation of the work by Tyagi *et al.* (2007). However, they did not analyse the role of non-normality in thermoacoustic interactions. In this paper, the effects of non-normality and nonlinearity are separated analytically, shedding light on the role played by non-normality which has not been discussed previously.

2. Non-normality and transient growth of thermoacoustic oscillations

An operator is said to be non-normal if it does not commute with its adjoint (Schmid & Henningson 2001). Such an operator has non-orthogonal eigenvectors and this property leads to transient growth of oscillations before they eventually decay. This property is illustrated in figure 1, where e_1 and e_2 represent the direction of the eigenvectors and Φ is a vector in the functional space, which is expressed as a linear combination of the eigenvectors. Figure 1(*a*) shows that, for a normal system, Φ decreases monotonically if the amplitudes of the individual eigenvectors themselves decay. On the contrary, for the non-normal system shown in figure 1(*b*),

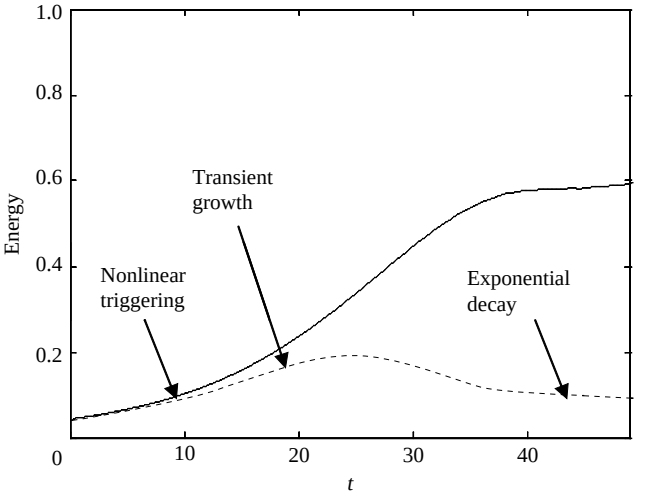

FIGURE 2. The evolution of non-dimensional acoustic energy $(1/2p'^2/(\gamma M)^2 + 1/2u'^2)$ obtained from ---, linear and ——, nonlinear simulations. $\eta_1(0) = 0.5$, $\dot{\eta}_1(0) = 0.5$, $x_f = 3/4$, $\alpha = 0.25$, $L_a/2H = 12.5$, $X_i = 3.2$, $Y_i = 3.2/7$ and $Pe = 5.0$.

Φ increases even when the amplitudes of individual eigenvectors decay. However, Φ decays after a sufficiently long time if nonlinear effects do not become significant during the transient growth. There could be situations where the short-term growth of fluctuations can lead to significant amplitudes, where nonlinear effects could cause 'nonlinear driving' (figure 2). Such a scenario arises in the evolution of thermoacoustic oscillations.

The acoustic equations (the assumptions in deriving these equations and the details of non-dimensionalization are given in § 4) in the presence of a heat source can be written as:

$$\gamma M \frac{\partial u'}{\partial t} + \frac{\partial p'}{\partial x} = 0, \tag{1}$$

$$\frac{\partial p'}{\partial t} + \gamma M \frac{\partial u'}{\partial x} = (\gamma - 1)\gamma \frac{L_a}{c_0} \frac{\dot{Q}'}{\rho_0 c_0^2}. \tag{2}$$

In (2), the heat release rate is obtained from a combustion model. In this paper, the thin-flame-sheet model for combustion is used to calculate the heat release rate. The acoustic field is assumed to be one-dimensional, though the combustion model is two-dimensional. The combustion zone is much smaller compared to the duct length and hence the source of heat release rate in (2) can be treated as a compact source. The model considered here is similar to that of Tyagi *et al.* (2007). The details of this model are discussed in § 4. The oscillatory heat release rate depends on the velocity and pressure perturbation. Hence, the oscillatory heat release rate, when linearized can be written as $\dot{Q}' = R(x, \varepsilon_i)\gamma M u' + S(x, \mu_i)p'$, where R and S can be treated as a continuous function of x (which could even be sharply peaked at the flame location as in the case of a compact flame), ε_i and μ_i are parameters which affect the heat release rate. The heat release rate could have an explicit dependence on time as well.

Equations (1) and (2) can be recast in matrix form as:

$$\begin{bmatrix} \dfrac{\partial}{\partial t} & \dfrac{\partial}{\partial x} \\ \dfrac{\partial}{\partial x} - \dfrac{RL_a\gamma(\gamma-1)}{\rho_0 c_0^3} & \dfrac{\partial}{\partial t} - \dfrac{SL_a\gamma(\gamma-1)}{\rho_0 c_0^3} \end{bmatrix} \begin{bmatrix} \gamma M u' \\ p' \end{bmatrix} = 0. \tag{3}$$

The matrix in (3) is a matrix of operators. The above operator does not commute with its adjoint for non-zero R and S. (The adjoint of a real matrix is simply the transpose of the matrix. The adjoint of a differential operator is its negative.) Therefore, it is clear that the thermoacoustic interaction is non-normal. In the absence of heat release, the matrix is symmetric and hence normal.

The heat release rate for a diffusion flame is calculated using the Burke–Schumann model in this paper. The heat release rate is obtained by solving for the Schvab–Zeldovich variable, which is governed by an advection–diffusion equation. It has been shown that the advection–diffusion operator is non-normal (Reddy & Trefethen 1994; Trefethen 1997).

As a result of the non-normal behaviour, the solutions exhibit large transient growth which could potentially trigger nonlinearities in the system when the amplitudes reach high enough values. Under such circumstances, classical linear stability analysis becomes a poor indicator of system stability (Trefethen *et al.* 1993). This phenomenon has been studied in detail in the context of turbulence by Baggett, Driscoll & Trefethen (1995). They explain that in the non-normal evolution, the input and output structures (such as streamwise vortices, streaks, etc.) are different and nonlinearity closes the feedback loop by converting some of the output into input. In a similar manner, the interplay between transient linear growth resulting from non-normality and 'nonlinear mixing' can lead to the growth of the acoustic oscillations over a large number of cycles. The consequences of non-normality of modes have been studied in the context of instability of magnetic plasmas by Kerner (1989), the formation of cyclones by Farrell (1989) and transition to turbulence by Trefethen *et al.* (1993), Gebgart & Grossman (1994) and Baggett *et al.* (1995).

In order to analyse (3), the operator must be reduced to a finite-dimensional operator such as a finite-dimensional matrix. In this paper, the partial differential equations governing the combustion acoustic interaction are reduced to a set of ordinary differential equations using the Galerkin technique. This is achieved by decomposing the spatial variation using basis functions. This is similar to decomposing a vector along some basis. The basis functions used in this study are not the eigenmodes of the linearized system. Such an approach has been used in solving partial differential equations (see e.g. Henningson & Schmid 1992). The ODE obtained using this technique are in time domain. These evolution equations are solved numerically using the fourth-order Runge–Kutta scheme. This system of nonlinear ODEs is similar to the numerous dynamical systems in literature. Such systems show dynamical behaviour such as fractals and folds. The complete evolution equations are linearized and the linearized equations are found to be non-normal. It must be emphasized that the eigenvalues of the linearized equations are not the wavenumbers of the basis functions used in the Galerkin technique.

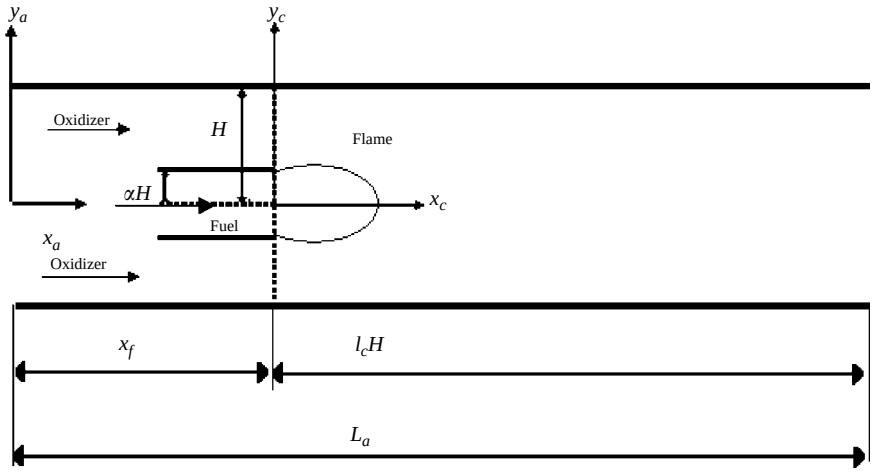

FIGURE 3. The burner configuration and the domain for acoustics and combustion. The flame is located at x_f. The origin and coordinate system of the combustion domain is denoted by subscript 'c' and that of the acoustic field is denoted by subscript 'a'.

3. The combustion model

The infinite-rate chemistry flame model is employed to study the unsteady two-dimensional co-flow non-premixed combustion. Figure 3 shows the geometry of the burner; the middle slot carries fuel and the outer slots carry oxidizer. This is identical to the geometry used by Tyagi *et al.* (2007). This model is similar to that considered by Buckmaster (2002) and is referred to as the thermodiffusive model by Kurdyumov & Matalon (2004); it is often adopted to investigate physical aspects specific to non-premixed combustion. The following assumptions have been made in deriving the model equations.

(i) The combustion length scale is negligible compared to the acoustic length scales and hence the spatial gradient in the velocity in the combustion zone is neglected.

(ii) The velocity field within the combustion zone is treated as a one-dimensional uniform field. The variation in density is neglected and an average value of density is assumed throughout.

(iii) The fuel and the oxidizer react as soon as they come in contact, as the reaction rate is much faster (infinite) when compared to the diffusion or convection rates. Hence, the flame at any instant will be located at the stoichiometric surface, where the Schvab–Zeldovich variable vanishes.

(iv) Lewis number is assumed to be 1.

This model is an extension of the classical Burke–Schumann model where, the unsteady effects are not considered.

The unsteady governing equation for Schvab–Zeldovich variable in the non-dimensional form is given by:

$$\frac{\partial Z}{\partial t} + u(t)\frac{\partial Z}{\partial x} = \frac{1}{Pe}\left(\frac{\partial^2 Z}{\partial x^2} + \frac{\partial^2 Z}{\partial y^2}\right), \tag{4}$$

where $u(t)$ is the net velocity in the combustion zone, Pe is the Péclet number ($u_0 H/D$, where D is the diffusivity of X and Y). A detailed derivation of this equation is given in Tyagi *et al.* (2007). The velocity used in (4) is the net velocity (sum of the base flow velocity and the fluctuating component of velocity), i.e. $u(t) = 1 + u'(t)$.

Schvab–Zeldovich variable is the difference in the non-dimensional oxidizer and fuel mass fractions ($Z = X - Y$). X is the oxidizer concentration non-dimensionalized by $\nu_x W_x$ and Y is the fuel concentration non-dimensionalized by $\nu_y W_y$, where W_x and W_y are the molecular masses of species X and Y, ν_x and ν_y are the stoichiometric coefficients of species X and species Y in the single-step reaction $\nu_x X + \nu_y Y \rightarrow$ Products. Following Tyagi *et al.* (2007), the variables in the above equation are non-dimensionalized using $x = \tilde{x}/H, \quad y = \tilde{y}/H, \quad t = (u_0/H)\tilde{t}, \; u = \tilde{u}/u_0$, where H is the half-duct width, u_0 is the velocity of the undisturbed flow, and the tilde denotes a dimensional quantity. The half-duct width is a measure of the combustion length scale, whereas the duct length is a measure of the acoustic length scale. The flame sheet is located at the $Z = 0$ surface (stoichiometric level surface). It is assumed that the fuel and oxidizer inlet ports are rectangular with the middle slot carrying the fuel and the outer two slots carrying the oxidizer. Hence, Z must satisfy the following boundary conditions (Chung & Law 1984):

(i) At the walls, $y = \pm 1$, $\dfrac{\partial Z}{\partial y} = 0$, $0 \leqslant x < l_c$

(ii) At the root of the flame, $x = 0$

$$Z = -Y_i, \quad -\alpha \leqslant y \leqslant \alpha,$$

$$Z = X_i, \quad -1 \leqslant y \leqslant -\alpha, \quad \alpha \leqslant y \leqslant 1,$$

(ii) At the exit of the duct, $x = l_c$, $\dfrac{\partial Z}{\partial x} = 0$

where, l_c is the non-dimensional distance between the duct end and the flame location, and X_i and Y_i are the non-dimensional oxidizer and fuel mass fractions at the inlet, respectively. Since the combustion zone is much smaller compared to the acoustic length scale ($2H/L_a \ll 1$), the outflow condition can be applied at infinity (Tyagi *et al.* 2007). However, in the present paper, the outflow conditions are applied at the duct end. The above boundary conditions must be supplemented by an initial condition. In this paper, it is assumed that a steady Burke–Schumann flame is perturbed initially which leads to unsteady combustion oscillations. It is possible to model the flame using other physical boundary conditions such as flux boundary condition which was used by Tyagi *et al.* (2007). In the present analysis, the boundary conditions by Chung & Law (1984) are used.

The above equation is solved using the Galerkin technique (Meirovitch 1967) and the solution can be written as,

$$Z = \sum_m \sum_n \cos(n\pi y) \sin\left(\left(m + \tfrac{1}{2}\right)\frac{\pi x}{l_c}\right) G_m^{(n)}(t) + Z_{st}, \tag{5}$$

where Z_{st} is the solution of steady Burke–Schumann equation (see Appendix B). The Galerkin technique makes use of the fact that any function in a domain can be expressed as a superposition of expansion functions which form a complete basis in that domain. The basis functions are chosen such that they satisfy the boundary conditions. However, the choice of the basis functions is not unique. The basis functions chosen here are just an arbitrary basis and not the eigenfunctions of the system. Clearly, the expansion functions chosen here satisfy the boundary conditions and they form a complete basis.

Substituting the expression for Z in (4), and projecting along the basis functions†, the following evolution equation for $G_m^n(t)$ is obtained,

$$\dot{G}_m^{(n)} + u(t)\sum_k W_{mk} G_k^{(n)} = -\frac{\left(m+\frac{1}{2}\right)^2\pi^2}{l_c^2 Pe} G_m^{(n)} - \frac{n^2\pi^2}{Pe} G_m^{(n)} + [u(t)-1]\, C_m^{(n)}, \quad (6)$$

where

$$C_m^{(n)} = -\int_0^{l_c}\int_{-1}^{1} \frac{\partial Z_{st}}{\partial x} \sin\left(m+\tfrac{1}{2}\right)\frac{\pi x}{l_c} \cos(n\pi y)\, \mathrm{d}y\, \mathrm{d}x,$$

$$W_{mk} = \left(k+\tfrac{1}{2}\right)\frac{\pi}{l_c}\int_0^{l_c} \sin\left[\frac{\left(m+\frac{1}{2}\right)\pi x}{l_c}\right] \cos\left[\frac{\left(k+\frac{1}{2}\right)\pi x}{l_c}\right] \mathrm{d}x$$

$$= \left[\frac{1-\cos(m+k+1)\pi}{2(m+k+1)} + \frac{1-\cos(m-k)\pi}{2(m-k)}\right]\left(k+\tfrac{1}{2}\right). \quad (7)$$

It can be seen from (6) that the evolution equations for the amplitude of the mth basis function depends on the amplitude of the kth Galerkin mode. Further, it can be seen from (7) that the dependence of the amplitude of the mth Galerkin mode on the amplitude of the kth Galerkin mode is different from the dependence of the kth Galerkin mode on the mth Galerkin mode. In other words, the matrix W does not commute with its adjoint. Hence, the evolution equations are non-normal. The eigenvectors of non-normal matrices are not orthogonal and hence the amplitude of each mode depends on the amplitude of other modes. Equation (6) can be written as a first-order matrix differential equation by considering only a finite number of Galerkin modes as follows:

$$\dot{\tilde{G}}^{(n)} + u(t)[W]\tilde{G}^{(n)} = -[D]^{(n)}\tilde{G}^{(n)} - C^{(n)}\,[u(t)-1]\,, \quad (8)$$

where, $\tilde{G}^{(n)} = \left[G_1^n\ G_2^n\ G_3^n \cdots G_M^n\right]^T$; $[D]_{mm}^{(n)} = -\dfrac{1}{Pe}\,\mathrm{diag}\left(\left(m+\tfrac{1}{2}^2\right)\dfrac{\pi^2}{l_c^2} + n^2\pi^2\right)$, (9)

and the elements of the matrix W are shown in (7). The first-order matrix differential equation can be solved analytically if the velocity profile at the flame is prescribed. The solution can be written as,

$$\tilde{G}^{(n)}(t) = \tilde{G}^{(n)}(0) - IF^{-1}(t)\int_0^t IF(t')\tilde{C}^{(n)}[u(t')-1]\,\mathrm{d}t'. \quad (10)$$

$\tilde{G}^{(n)}(0) = 0$ for an initially steady flame. $IF(t)$ is the integrating factor of the first-order matrix differential equation

$$IF(t) = \exp\left[[W]\int_0^t u(t')dt'\right]\exp[D]t.$$

It can be inferred from the solution that Z has exponential dependence on the amplitude of acoustic perturbations and hence the combustion response to external velocity perturbations is nonlinear even though the evolution equations are linear. It will be shown in § 4 that, in a self-excited system where the combustion oscillations and acoustic oscillations are coupled, the evolution equations themselves are nonlinear.

† The component or the projection of a function f along a basis function ψ_n is given by their inner product $\langle f\,|\psi_n\rangle$ which is defined as $\int_{domain} f(x)\psi_n(x)\,\mathrm{d}x$.

The evolution equations when linearized yield non-orthogonal eigenvectors which lead to transient growth. The coupled response will be discussed in detail in the next section.

It is necessary to calculate the heat release rate to study the coupled response and it can be done as follows (Tyagi *et al.* 2007). The Burke–Schumann temperature field (non-dimensionalized by Q_H/C_p) is given by:

$$T_{bs} = T_i + X_i(Y_i + Z)/(X_i + Y_i) \text{ for } Z \leqslant 0;\ T_{bs} = T_i + Y_i(X_i - Z)/(X_i + Y_i) \text{ for } Z \geqslant 0, \tag{11}$$

where, T_i is the non-dimensional inlet temperature, and Q_H is the heating value of fuel per unit mass of the mixture. The above expression for temperature is an exact solution of the energy equation in the infinite reaction rate assumption and for Dirchlet boundary conditions for both energy and Z equations, if the pressure oscillations are negligible. This happens when the Mach number of the mean flow is very low. The heat release rate can then be calculated from the temperature field using thermodynamic relations (Tyagi *et al.* 2007). In deriving the expression for the temperature field, the effect of pressure oscillations are assumed to be negligible when compared to the effects of convection, diffusion and reaction in the infinite-rate chemistry assumption. This is shown in Appendix A. The heat release rate (non-dimensionalized by the heating value of fuel) is given by,

$$\dot{Q}_c = \int_V \left(\frac{\mathrm{d}T_{bs}}{\mathrm{d}t} + T_{bs} \nabla \cdot \boldsymbol{u} \right) \mathrm{d}V = \int_V \left(\frac{\partial T_{bs}}{\partial t} + \nabla \cdot (T_{bs} \boldsymbol{u}) \right) \mathrm{d}V, \tag{12}$$

where $\boldsymbol{u}$ is the net velocity in the combustion domain and it is directed along the length of the duct. The average heat release rate is given by,

$$\begin{aligned} \dot{Q}_{av} &= \sum \sum \frac{\mathrm{d}G_m^{(n)}}{\mathrm{d}t} (R_{nm}) + \sum \sum u(t) G_m^{(n)} J_{nm} + Q_{st}\,(u(t) - 1) \\ &= [R] \frac{\mathrm{d}\bar{G}}{\mathrm{d}t} + u(t)\,[J]\,\bar{G} + Q_{st}\,(u(t) - 1)\,, \end{aligned} \tag{13}$$

where $\bar{G} = [\tilde{G}^{(1)}\ \tilde{G}^{(2)}\ \tilde{G}^{(3)} \cdots \tilde{G}^{(n)} \cdots \tilde{G}^{(N)}]^T$,

$$R_{nm} = \int_0^{l_c} \int_{-1}^{1} \left[\theta(-Z) \frac{Y_i}{X_i + Y_1} - \theta(Z) \frac{X_i}{X_i + Y_1} \right] \sin\left(\frac{m + \frac{1}{2}}{l_c} \pi x \right) \cos(n\pi y)\ \mathrm{d}y\,\mathrm{d}x,$$

$$J_{nm} = \int_{-1}^{1} \left[\theta(-Z(l_c, y)) \frac{Y_i}{X_i + Y_1} - \theta(Z(l_c, y)) \frac{X_i}{X_i + Y_1} \right] (-1)^m \cos(n\pi y)\ \mathrm{d}y,$$

and θ is the step function. The dependence of $\tilde{G}(n)$ on the imposed velocity is given by (10). In this case, it is assumed that the velocity field is prescribed as a function of time and it is independent of the combustion process. We would like to emphasize that when there is feedback from the acoustic field, the acoustic velocity will depend on $\tilde{G}(n)$. This coupling between the acoustic field and the combustion zone is discussed in the next section. However, it can be seen from the above equation that the heat release rate is a nonlinear function of the acoustic variables, since $\tilde{G}(n)$ has exponential dependence on the velocity. As shown earlier, the combustion modes are non-normal, leading to the interaction between combustion modes. Since the combustion process interacts with the acoustic field, the interaction between combustion modes will lead to interaction between acoustic modes. The interaction

process is further complicated if nonlinear acoustics is considered. To focus attention on the non-normal and nonlinear behaviour of the combustion response, we have modelled the acoustic field using a one-dimensional linear acoustic model as in Tyagi *et al.* (2007).

4. Interaction between the combustion process and the acoustic field

In this section, coupled ordinary differential equations that describe the interaction between the combustion process and acoustic field are derived. Assuming a perfect, inviscid and non-heat-conducting gas, the governing equations for the one-dimensional acoustic field in the absence of mean flow and mean temperature gradient in the duct are (Tyagi *et al.* 2007):

Acoustic momentum:

$$\rho_0 \frac{\partial \tilde{u'}}{\partial \tilde{t}} + \frac{\partial \tilde{p}'}{\partial \tilde{x}} = 0, \tag{14a}$$

Acoustic energy:

$$\frac{\partial \tilde{p}'}{\partial \tilde{t}} + \gamma p_0 \frac{\partial \tilde{u}'}{\partial \tilde{x}} = (\gamma - 1)\, \dot{\tilde{Q}}', \tag{14b}$$

where, $\tilde{p}'$ is the acoustic pressure, $\tilde{u}'$ is the acoustic velocity and, $\dot{\tilde{Q}}'$ the unsteady heat release rate. The expression for $\dot{\tilde{Q}}'$ can be related to $\dot{\tilde{Q}}'_c$ through dimensional constants as $\dot{\tilde{Q}}' = \rho_0 c_p T_{ref}(u_0/H)\dot{\tilde{Q}}'_c$. The above equations can be non-dimensionalized as

$$\tilde{x} = L_a x; \quad \tilde{t} = (L_a/c_0)t; \quad \tilde{u}' = u_0 u'; \quad \tilde{p}' = p_0 p'; \quad M = (u_0/c_0);$$

where L_a is the length of the duct, the subscript '0' indicates quantities in the undisturbed medium. The time scale used to non-dimensionalize the combustion equation is H/u_0, whereas the time scale used to non-dimensionalize the acoustic equations is L/c_0.

The duct is assumed to be open at both ends and hence the acoustic pressure vanishes at the ends. The unsteady heat release is assumed to be a compact source; i.e. $2H/L_a \ll 1$ (Tyagi *et al.* 2007). Equations (14*a*) and (14*b*) can then be rewritten in the dimensionless form as,

$$\gamma M \frac{\partial u'}{\partial t} + \frac{\partial p'}{\partial x} = 0, \tag{15}$$

$$\frac{\partial p'}{\partial t} + \gamma M \frac{\partial u'}{\partial x} = (\gamma - 1)\gamma \frac{L_a}{c_0} \frac{\dot{\tilde{Q}}_{av}}{\rho_0 c_0^2} \frac{\delta(x - x_f)}{L_a}, \tag{16}$$

where $\dot{\tilde{Q}}_{av}$ is the heat release rate averaged over the combustion zone, and x_f is the flame location. Equations (15) and (16) are nonlinear as the heat release has a nonlinear dependence on the acoustic field.

The acoustic field is solved in the time domain using the Galerkin technique (Dowling 1995; Dowling & Stow 2003). The acoustic pressure and acoustic velocity can be written as:

$$u' = \sum_{j=1}^{N} \eta_j \cos(j\pi x), \quad p' = -\sum_{j=1}^{N} \frac{\gamma M}{j\pi} \dot{\eta}_j \sin(j\pi x). \tag{17}$$

The velocity used in (4) is the sum of acoustic velocity evaluated at the flame location x_f and the base flow. The Galerkin mode functions chosen for the acoustic variables satisfy the boundary conditions and form a complete basis as well. The basis functions are the eigenmodes of the self-adjoint part of the linearized operator, i.e. the natural modes of a duct in the absence of the flame. The following evolution equations for the acoustic field are obtained after substituting the expressions for acoustic velocity and pressure in the linear acoustic equations and integrating over the duct (domain for the acoustic field) after multiplying by the basis functions,

$$\frac{\mathrm{d}\eta_j}{\mathrm{d}t} = \dot{\eta}_j, \quad \frac{\mathrm{d}\dot{\eta}_j}{\mathrm{d}t} + k_j^2\eta_j = -\frac{2k_j\dot{Q}_{av}}{(T_i + T_{ad})/2}\sin(j\pi x_f), \tag{18}$$

where T_i is the inlet temperature, T_{ad} is the adiabatic flame temperature and k_j is the wavenumber corresponding to the jth Galerkin mode.

Further, the role of damping on the growth and saturation of oscillations is also studied. The damping model used in this paper is same as that considered by Matveev (2003). In the presence of damping, the above set of equations can be modified as follows:

$$\frac{\mathrm{d}\eta_j}{\mathrm{d}t} = \dot{\eta}_j, \qquad \frac{\mathrm{d}\dot{\eta}_j}{\mathrm{d}t} + 2\xi_j\omega_j\dot{\eta}_j + k_j^2\eta_j = -\frac{2k_j\dot{Q}_{av}}{(T_i + T_{ad})/2}\sin(j\pi x_f), \tag{19}$$

where the damping constant is given by:

$$\xi_j = \frac{1}{2\pi}\left[c_1\frac{\omega_j}{\omega_1} + c_2\sqrt{\frac{\omega_1}{\omega_j}}\right], \tag{20}$$

where ω_j is the wavenumber of the jth mode, ω_1 is the wavenumber of the first mode. Damping is higher for higher wavenumbers. Hence higher wavenumbers in the oscillations decay rapidly, when there is no mechanism to drive the higher wavenumber. Damping occurs owing to acoustic boundary-layer losses which are modelled as a volumetric source term and owing to sound radiation losses at the ends and convection of sound by the mean flow.

The expression for heat release rate in (12) can be written in matrix form as,

$$\begin{aligned}\dot{Q}_{av} &= \sum\sum\frac{\mathrm{d}G_m^{(n)}}{\mathrm{d}t}(R_{nm}) + \sum\sum u(t)G_m^{(n)}J_{nm} + Q_{st}(u(t)-1)\\ &= [R]\frac{\mathrm{d}\bar{G}}{\mathrm{d}t} + u(t)[J]\bar{G} + Q_{st}(u(t)-1),\end{aligned} \tag{21}$$

where $\bar{G}$, $[R]$ and $[J]$ are defined after (13). The nonlinearity in the heat release rate is due to the dependence of $\bar{G}$ on the fluctuating velocity (equation (8)). In this situation, when there is feedback, it is not possible to solve for the combustion field independently. The nature of combustion–acoustic interaction is determined by the set of equations in (8) and (18)–(19).

Equations (18)–(19) and (21) show that the advection velocity is a function of the amplitude of the combustion modes. This makes the advection term in (8) nonlinear. Hence, the coupled equations governing the combustion–acoustic interaction are nonlinear. Apart from being nonlinear, the combustion equations are also non-normal as discussed earlier. The coupled equations can be written in matrix form as follows:

$$M\frac{\mathrm{d}\chi}{\mathrm{d}t} + B_{NL}(\chi)\chi + B_{NN}\chi = 0, \tag{22}$$

where $\chi = [G_{M\times N}\ \varphi_{2K\times 2K}]^T$, $\varphi_{2K\times 2K} = [\eta_1\ \dot{\eta}_1 \ldots \eta_K\ \dot{\eta}_K]$. The expanded forms of the matrices are presented in Appendix B. The above system of equations is integrated using the fourth-order Runge–Kutta technique. In (22), B_{NL} is the matrix which leads to nonlinear interaction and B_{NN} is the matrix which leads to non-normal growth of the oscillations. This equation has the same form as that of the evolution equations discussed by Trefethen *et al.* (1993), Gebgart and Grossman (1994) and Baggett *et al.* (1995) and hence it is expected that the above system might show similar behaviour as discussed in these references.

Equation (22) when linearized yields:

$$M\frac{\mathrm{d}\chi}{\mathrm{d}t} + B_{NN}\chi = 0 \quad \text{or} \quad \frac{\mathrm{d}\chi}{\mathrm{d}t} = L\chi \text{ where } L = -M^{-1}B_{NN}. \tag{23}$$

In (23), L is called the stability matrix (Schmid & Henningson 2001) and it is purely non-normal. When the real part of all eigenvalues of matrix L is negative, the oscillations of the linearized system eventually decay. However, because of the non-orthogonality of the eigenvectors, it is possible for the linearized system to exhibit large transient growths triggering the nonlinearities as illustrated in figure 1. In the next section, we will use (23) to study the transient growth of the above system of equations and analyse the stability of combustion–acoustic interaction.

5. Transient growth

The thermoacoustic system described in § 4 has a non-normal evolution, which leads to transient energy growth. As discussed earlier, transient growth plays an important role in amplifying the initial disturbances to a value high enough that nonlinear effects can play a significant role. Hence, it is necessary to identify the initial conditions for which the transient growth is maximum. Schmidt & Henningson (2001) give a detailed discussion on the analysis of transient growth, in the context of transition to turbulence in shear flows. They analysed the stability of shear flows by studying the energy growth of the system. However, their analysis is quite general and can be applied to thermoacoustic systems as well. In this analysis, the development of a general solution of the linearized system is considered rather than the individual eigenmodes of the system. The evolution operator (matrix) of the coupled combustion–acoustic system described by (23) is non-normal as, $LL^{\dagger} \neq L^{\dagger}L$. The solution of this system can be written in the operator form as (Schmid & Henningson 2001)

$$\tilde{\eta}(t) = \exp(Lt)\tilde{\eta}(0) = S^{-1}\exp(L_D t)S\tilde{\eta}(0) \tag{24}$$

where, L is the stability operator, S is the similarity transformation that diagonalizes L, and L_D is the diagonal form of L. Since L is non-normal, S is non-unitary, indicating that it is not possible to make the eigenvectors perpendicular by a simple rotation or by a different choice of basis functions. The maximum amplification of the energy density is defined as the growth factor which is given by (Schmid & Henningson 2001),

$$G(t) = \max_{\tilde{\eta}(0)} \frac{\|\tilde{\eta}(t)\|^2}{\|\tilde{\eta}(0)\|^2} = \|\exp(Lt)\|^2, \tag{25}$$

where 'max' indicates that the ratio is maximized over all possible initial conditions. The initial condition $\tilde{\eta}(0)$ that maximizes the growth factor $G(t)$ is different for different times and hence the maximum growth (corresponding to this initial condition) is the envelope of the energy evolution of all possible initial conditions

(Schmid & Henningson 2001). The expression in (25) is maximized for various instants of times over all possible initial conditions. This is achieved through singular value decomposition. The initial condition corresponding to the maximum singular value is chosen as the initial condition leading to maximum growth rate. The maximum growth factor in a particular time interval $[0, t]$ is defined as $G_{max} = \max_t G(t)$.

If there exists an unstable eigenvalue, then the above maximum value is infinite. This corresponds to the linearly unstable system. The G_{max} values for various parameters are calculated and the regions with large transient growth are identified. The $G_{max} = 1$ contour separates parameter combinations for which transient growth may occur from those for which energy decay must occur. When $G_{max} = 1$, then the energy at any instant is less than the initial energy of the system and when $G_{max} > 1$, the system will exhibit transient growth. Hence, a system which is linear to begin with will behave like a linear system throughout its evolution as there is no amplification of the oscillations to trigger nonlinear effects, when $G_{max} = 1$. This enables us to study the range of parameters for which the system is linearly stable, linearly unstable and the region where transient growth is significant.

6. Pseudospectra

If a linear operator is normal, then the degree of resonant amplification that may occur in response to an input frequency is inversely proportional to the distance in the complex plane between the input frequency and nearest eigenvalues. However, for a non-normal operator, the resonant amplifications may be orders of magnitude greater (Trefethen *et al.* 1993). The resonances of a non-normal system are not determined by the eigenvalues alone. Such a resonance of a non-normal system is known as pseudoresonance.

The concept of ε-pseudoeigenvalues can be used to analyse the behaviour of evolution governed by such non-normal operators (Trefethen & Embree 2005). z is an ε-pseudoeigenvalue of A if it satisfies $\|(zI - A)^{-1}\| \geqslant \varepsilon^{-1}$. There are other equivalent definitions of pseudoeigenvalues and they have been discussed in detail by Trefethen & Embree (2005). The geometry of pseudospectra reveals information about transient growth factor and the non-normal nature of the operator. The pseudospectra of normal operators are closed circles. When a contour corresponding to some ε value does not lie entirely in the left half-plane, the system exhibits transient growth, causing the amplitudes to increase to high values (Trefethen *et al.* 1993). Further, it is possible to obtain necessary and sufficiency conditions for an oscillation to be stable based on the geometry of pseudospectra. These conditions are presented in § 7.

7. Results and discussion

The acoustic modes are normal in the absence of combustion. However, the presence of combustion makes the system non-normal, as can be seen from the following physical arguments. A small disturbance in velocity causes the combustion process to become unsteady and it in turn acts as the source of acoustic oscillations. The acoustic field in a duct is driven by combustion when the combustion oscillations are in phase with the acoustic oscillations. The phase lag between the two processes itself evolves with time and hence the phase difference between the combustion and the acoustic oscillations depends on the phase difference between the two processes at an earlier time. Combustion drives that mode of acoustics which is in phase with the combustion process. Since the phase difference between the combustion and a

particular mode of the acoustic field depends on the phase difference at an earlier time, the interaction would depend on that mode of the acoustic field which was in phase with combustion at an earlier time. Hence, the mode which is excited at a particular instant of time depends on which mode was excited at an earlier time. In general, this would lead to a complicated interaction between various modes, which would lead to non-orthogonal behaviour of the eigenmodes. This is the defining characteristic of non-normal systems.

The non-normality of the combustion process is present even in the absence of the feedback from the acoustic field. This is because the non-normality in the combustion process is due to convection, which transports heat from a 'hot' region to a region which is colder. This process is different from diffusion; diffusion is a gradual process in which the direction of transport is the same as the direction of the thermal gradient, unlike convection in which it is the direction of the flow. Hence the base flow convects heat from a hot region to a cold region where the relative amplitude of the heat release oscillations increases. This causes interaction among various combustion modes. Hence, it can be seen that the eigenmodes are non-orthogonal in this case as well, as two different oscillatory modes, i.e. the oscillatory conduction and the oscillatory convection, are interdependent. This behaviour is analogous to the kind of behaviour in vortical flows that leads to formation of streaks (Trefethen *et al.* 1993) at the onset of transition to turbulence. The feature discussed above can also be thought of as an entropy wave as entropy is convected with the flow.

$$T\left[\frac{\partial s}{\partial t}+u(t)\frac{\partial s}{\partial x}\right]=-\frac{1}{Pe}\left[\frac{\partial^2 s}{\partial x^2}+\frac{\partial^2 s}{\partial y^2}\right]+Q\delta(Z). \tag{26}$$

The flame sheet acts as a localized source of entropy disturbance, and (26) describes the propagation of this disturbance to other regions in space. The entropy disturbance propagates with the flow velocity and also diffuses to other regions. This movement of entropy disturbance is similar to the advection of vorticity disturbance in shear flows causing the occurrence of structures such as streaks (Trefethen *et al.* 1993). The non-normality of the combustion process is essentially due to the movement of entropy disturbances from regions of high entropy to low entropy. The advection of entropy disturbances causes the various eigenmodes of the system to be interrelated, thereby making it non-normal.

Balasubramanian & Sujith (2007) studied triggering of thermoacoustic instabilities in a Rijke tube. In this paper, a correlation for the heat release rate given by Heckl (1990) was used instead of solving the advection–diffusion equation. This simplified approach was followed in order to focus on the non-normal nature of the acoustic equations alone in the presence of heat source. This study showed that the presence of a heat source makes a thermoacoustic system non-normal, even though the thermal modes were not considered.

The effect of non-normality on the evolution of a thermoacoustic system is presented in the following subsections. Test numerical simulations were performed for different choices for the number of acoustic and combustion modes used in the Galerkin technique and the number of modes was chosen (for subsequent simulations) such that the change in the solution is within 5%, if additional modes are introduced. It was observed that 900 combustion modes (30 for y-dependence and 30 for x-dependence) and 4 acoustic modes are sufficient. To be conservative, 2500 combustion modes (50 for the y-dependence and 50 for x-dependence) and 6 acoustic modes were taken for the calculations presented subsequently.

7.1. *Triggering of nonlinearities*

If the system is non-normal as well as nonlinear, oscillations can grow even when the individual eigenvalues indicate linear stability. For such systems, there exists some initial condition for which the oscillations decay and some initial conditions for which the oscillations grow. In this example, this feature is captured by a flame located at 3/4 duct length when the fuel slot width is 0.25. The Péclet number was chosen as 5.0, X_i was chosen as 3.2, Y_i was chosen as 3.2/7 and the duct length to duct width ratio was chosen as 25.0. For reasons that will become clear later, damping is assumed to be absent in this example. The initial conditions chosen are $\eta_1(0) = 0.1$, $\eta_{i\neq 1}(0) = 0$ and $\dot{\eta}_i(0) = 0$. Figures 4(*a*) and 4(*b*) show that the oscillations decay even though there are several periods of short time growth. This indicates that in this case, transient growth is not sufficient to trigger the nonlinearities. Figure 4(*c*) shows the variation of heat release rate with velocity, also known as the phase portrait. The phase portrait is elliptically spiralling inwards, which indicates that the response of heat release rate to velocity fluctuations is almost linear. The elliptical nature also indicates that there is a phase difference between the heat release rate and the velocity perturbations.

Figure 5(*a*) shows that for the same thermoacoustic system, for a different initial condition, i.e. $\eta_1(0) = 0.5$, $\dot{\eta}_1(0) = 0.5$, $\eta_{i\neq 1}(0) = 0$ and $\dot{\eta}_{i\neq 1}(0) = 0$ the oscillation grows and saturates. The evolution of the non-dimensional acoustic energy $(1/2p'^2/(\gamma M)^2 + 1/2u'^2)$ after locally weighted regression smoothing (LOWESS) has been calculated from both linear and nonlinear simulations and is presented in figure 2. This is a measure of the average acoustic energy in a cycle. The results of linear simulation are obtained by solving the linear system of equations in (23). The results of the nonlinear simulation are obtained by solving the system of equations in (22). Linear simulation shows that the acoustic energy grows for a short time and then decays. Nonlinear simulation is almost identical to the linear simulation initially. After sufficient transient growth, the nonlinearity 'picks up' which can be seen from the deviation of the nonlinear evolution from the linear evolution. Figure 5(*b*) shows that after some time the mean value of heat release rate changes with time, indicating nonlinear behaviour. The nonlinear response of the heat release rate can also be seen from the fractal behaviour exhibited by the phase portrait shown in figure 5(*c*) which shows folds similar to Rossler bands. Such fractal behaviour, known as folds, has been discussed in the context of premixed flames by Fichera, Losseno & Pagano (2001).

Another interesting feature shown by the system is saturation in the absence of damping. It is known from the Rayleigh criterion that there is acoustic driving when the instantaneous acoustic pressure is in phase with the instantaneous value of heat release rate. The phase $\phi(t)$ between the pressure and heat release oscillations at any instant is defined as

$$\cos\phi(t) = \int_0^t p'(t')Q'(t')\,\mathrm{d}t' \Big/ \sqrt{\int_0^t p'^2(t')\,\mathrm{d}t'}\sqrt{\int_0^t Q'^2(t')\,\mathrm{d}t'}.$$

The above expression is the correlation between pressure and heat release rate signals. Saturation can occur when the phase difference between the pressure oscillations and the heat release rate becomes 90° (W. Polifke, personal communication 2006). When the heat release rate and pressure oscillations differ by a phase of 90° then, at that time instant, the growth rate of energy is zero and hence further growth is not possible. Hence when the phase difference becomes 90° and if it remains a constant, then the oscillations will saturate. This can be inferred from figure 5(*d*) which shows the

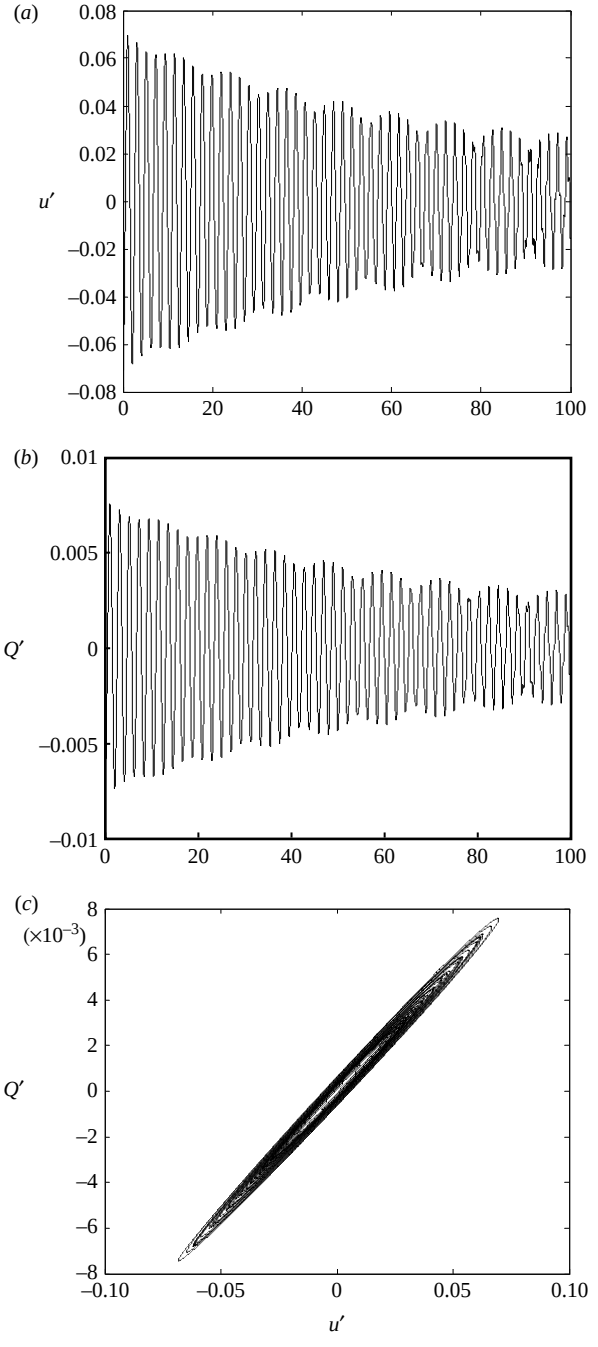

FIGURE 4. The evolution of (*a*) acoustic velocity, (*b*) heat release and (*c*) phase portrait at the flame location for a case where the initial condition corresponds to excitation of the first duct mode; $\eta_1(0) = 0.1$; $x_f = 3/4$; $Pe = 5.0$, $X_i = 3.2$, $Y_i = 3.2/7$, $\alpha = 0.25$ and $L_a/(2H) = 25$.

evolution of phase difference to 90° as the oscillation saturates. Saturation of the oscillations also indicates the existence of an attractor (as the system tends towards a limit-cycle operation) and the fractal dimension of the attractor is found to be 1.68. The fractal dimension is obtained using a box-counting technique. There are various

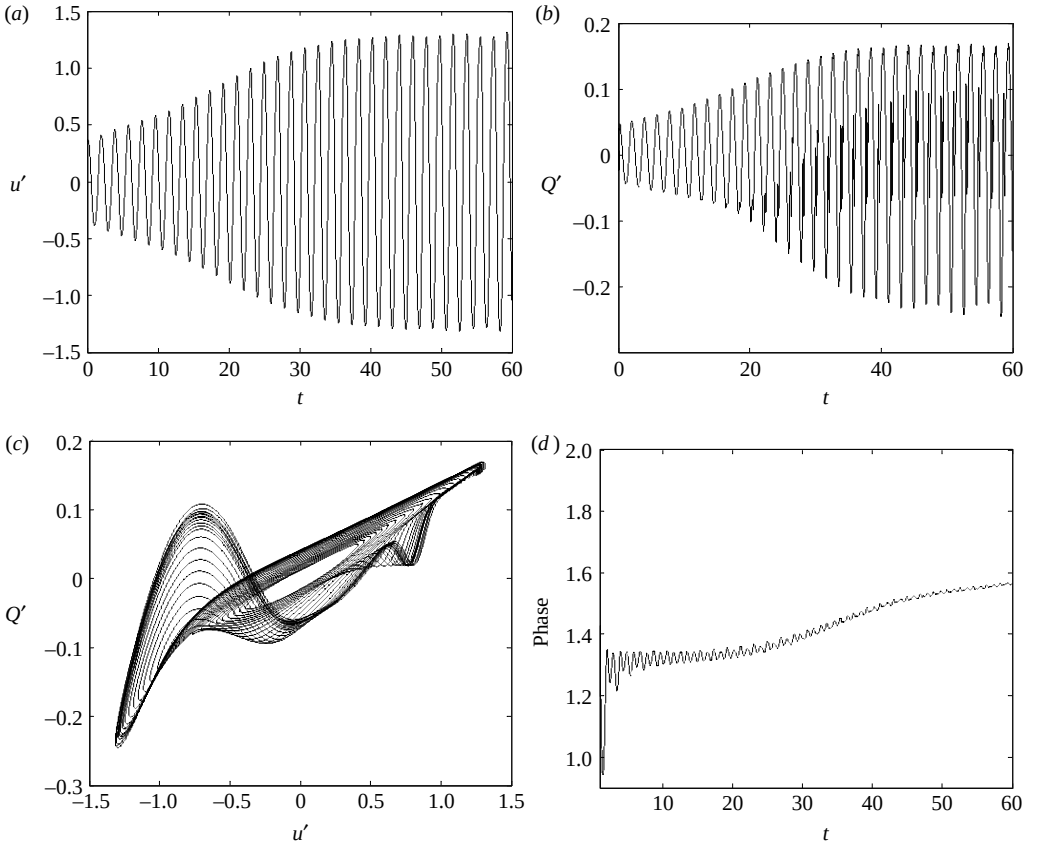

FIGURE 5. (*a*) Evolution of acoustic velocity at the flame location; (*b*) heat release evolution and (*c*) phase portrait for a case with the initial condition $\eta_1(0) = 0.5$, $\dot{\eta}_1(0) = 0.5$. (*d*) The evolution of the phase difference (in radians) between heat release and acoustic pressure to $\pi/2$ as the amplitude saturates. $x_f = (3/4)$ $Pe = 5.0$, $X_i = 3.2$, $Y_i = 3.2/7$, $L_a/2H = 25$.

definitions of fractal dimension; here we have referred to the box-counting dimension as the fractal dimension. (The box-counting dimension is given by $D_B = \lim_{\delta \to 0}[\log(N)/\log(1/\delta)]$ where N is the number of boxes of side length δ used to cover the attractor and is calculated by calculating the slope of the $\log(N)$–$\log(1/\delta)$ plot).

Wicker *et al.* (1996) define triggering combustion instability in the context of their study of combustion instabilities in rocket motors as 'initiation of unstable pressure oscillations by a finite amplitude pulse in a system that is otherwise stable to small perturbations'. The studies of Culick, Burnley & Swenson (1995) Wicker *et al.* (1996), and Anathkrishnan, Deo & Culick (2005) have attributed triggering to nonlinear combustion. These studies include the effect of nonlinear acoustics as well, although they state that nonlinear acoustics alone is insufficient to cause triggering. The present study highlights the role of non-normality in the occurrence of triggering combustion instabilities. The transient growth arising because of the non-normality of the thermoacoustic system triggers nonlinearities when the amplitude reaches high enough values, resulting in further growth of the oscillations.

7.2. *Growth of oscillations in an initially decaying system*

This section discusses bootstrapping in a thermoacoustic system which is stable according to classical linear stability analysis based on eigenvalues. In this example, the flame is located at 1/4 duct length and the fuel slot width is 1/4. The Péclet number was chosen as 10.0, X_i was chosen as 3.2/7, Y_i was chosen as 3.2 and the duct length to duct width ratio was chosen as 12.5. The initial conditions chosen are $\eta_1(0) = 0.1$, $\eta_{i\neq1}(0) = 0$ and $\dot{\eta}_i(0) = 0$.

Figure 6(*a*) shows that although the low-frequency oscillations that are initially excited in the system decay, high-frequency oscillations sets in after some time. It must be emphasized that classical linear stability analysis based on the eigenvalues shows all eigenmodes of the coupled system to be stable.

If the eigenmodes are orthogonal, there is no energy exchange between them. However, for a non-normal system, the eigenmodes are non-orthogonal, and energy can be redistributed among the various modes owing to the interaction of the modes with the base flow. Although the basis functions used in the Galerkin expansion are orthogonal, they are related to the eigenmodes using a non-orthogonal transformation, as the system is non-normal. This results in an exchange of energy projected into the Galerkin functions.

Figure 6(*b–d*) shows the evolution of the energy projected on the first three Galerkin expansion functions. It can be seen that while the energy projected to the first expansion function decays, the projection on the second and third expansion functions grow. After sufficient energy is projected onto the second and third expansion functions, they project energy back, causing the energy projected on the first expansion function to grow. This bootstrapping results in a shift in frequency during the evolution. The net effect of all these energy transfers causes the acoustic velocity to grow and eventually saturate. This feature has been discussed in the context of turbulence and it is known as 'bootstrapping' (Gebgart & Grossman 1994; Baggett *et al.* 1995). Yoon, Peddieson & Purdy (2001) have discussed 'bootstrapping' in the context of a Rijke tube using an *ad hoc* nonlinear model for the heat release rate.

Figures 6(*e*) and (*f*) show the heat release rate spectra for $0 < t < 9$ and $9 < t < 60$, respectively. (In these plots, ω is the non-dimensional frequency.) The dominant frequency during the period $0 < t < 9$ dies and is absent for $9 < t < 60$. It can be seen that there are several peaks in the second part of the evolution, indicating the generation of higher frequencies. The dominant non-dimensional frequency is 1.38 in the second part of the evolution. This frequency does not correspond to any natural frequency of the duct. This feature of combustion instabilities occurring at frequencies that are far from the natural acoustic frequencies was discussed in the context of dump combustors by Matveev & Culick (2003) and experimentally observed by Schadow *et al.* (1989). Figure 6(*g*) shows the flame shape at different instants of time during the limit cycle. Figure 6(*h*) shows the corresponding non-dimensional acoustic velocity in the combustion zone. It can be seen that the flame shape oscillates with the acoustic velocity, with the flame periodically elongating and contracting without wrinkling. This results in the oscillation in heat release rate. Further, it can be seen that the time-averaged flame shape is not the same as the steady Burke–Schumann flame; the time–averaged flame is longer than the steady flame.

The occurrence of harmonic frequency generated by oscillating flames was experimentally observed by Lang (1991). The generation of higher harmonics is usually attributed to the nonlinear nature of the interaction. However, there can be

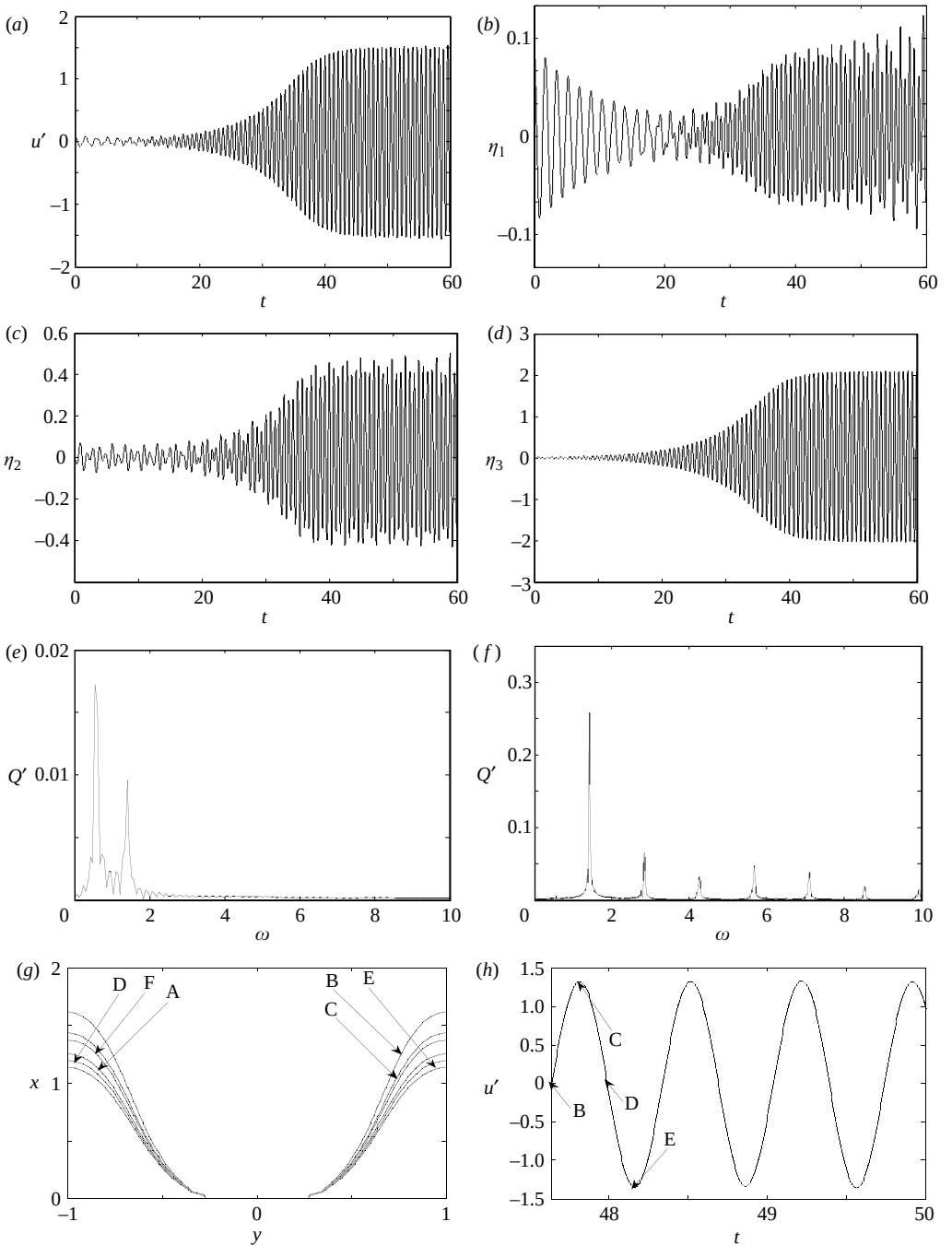

FIGURE 6. (*a*) The evolution of acoustic velocity at the flame location with time. (*b–d*) The projection of the acoustic velocity onto the Galerkin modes. (*e*, *f*) The heat release rate spectra for the period $0 < t < 9$ and $9 < t < 60$, respectively. (*g*) The flame shapes at various instants. (*h*) The velocity at those time instants. The contour marked as A is the steady Burke–Schumann flame and the contour marked F is the time-averaged flame shape. $\eta_1(0) = 0.1$, $\dot{\eta}_1(0) = 0.1$. $L_a/2H = 12.5$, $X_i = 3.2/7$, $Y_i = 3.2$, $\alpha = 0.25$, $Pe = 10$.

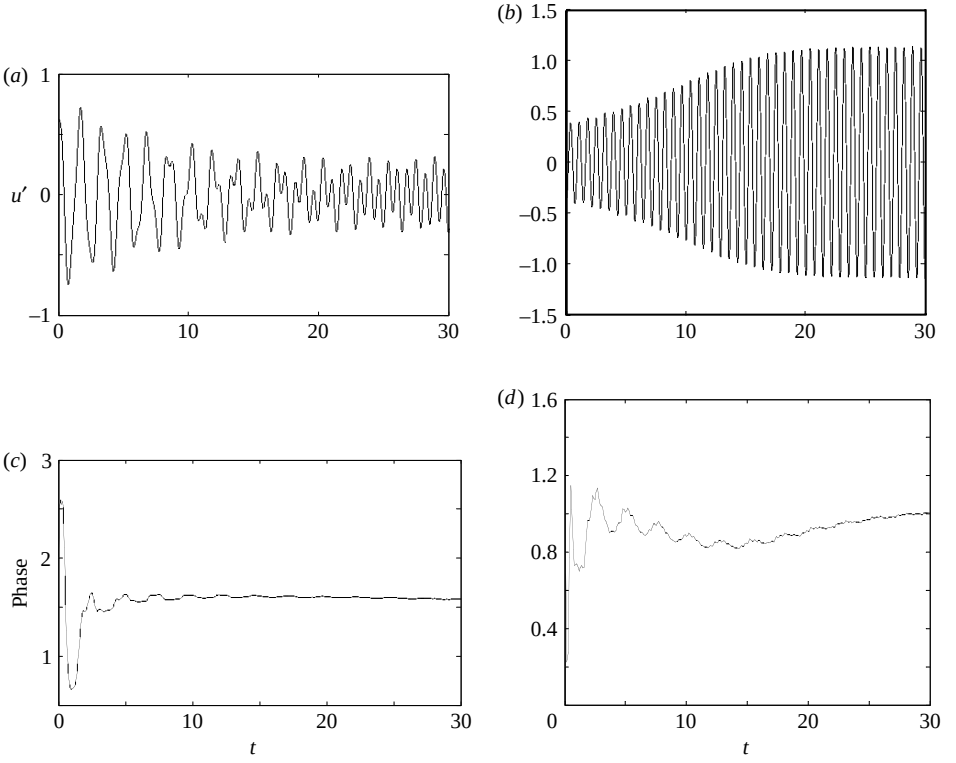

FIGURE 7. (*a*) Evolution of acoustic velocity at the flame location for a case with the initial condition $\eta_1(0) = 0.5$, $\eta_3(0) = 0.5$, $\eta_{i\neq1,3}(0) = 0$ and $\dot{\eta}_i(0) = 0$; (*b*) evolution of acoustic velocity, for a case with the initial condition $\eta_3(0) = 0.5$, $\eta_{i\neq3}(0) = 0$ and $\dot{\eta}_i(0) = 0$; (*c*, *d*) evolution of phase between heat release and acoustic pressure $x_f = 1/4$, $Pe = 10.0$, $X_i = 3.2/7$, $Y_i = 3.2$, $L_a/2H = 12.5$, $c_1 = 0.015$, $c_2 = 0.001$.

redistribution of energy in two ways. The first is a nonlinear mechanism where two individual eigenmodes interact directly causing exchange of energy between the two modes. Another mechanism which causes redistribution of energy is the interaction of various eigenmodes with the base flow. At lower amplitudes when nonlinear effects are insignificant, redistribution of energy occurs mainly because of the interaction of the various modes with the base flow.

7.3. *Effect of damping*

The effect of damping on the non-normal nature of the system is studied in this example. The damping coefficients c_1 and c_2 are taken to be 0.015 and 0.001, respectively. The evolution of the acoustic field for two different initial conditions is studied for a system whose eigenvalues indicate linear stability. The slot width is taken to be 0.25. Figure 7(*a*) shows the evolution of acoustic velocity for the initial condition $\eta_1(0) = 0.5$, $\eta_3(0) = 0.5$, $\eta_{i\neq1,3}(0) = 0$ and $\dot{\eta}_i(0) = 0$. Figure 7(*b*) shows the evolution of acoustic velocity for the initial condition $\eta_3(0) = 0.5$, $\eta_{i\neq3}(0) = 0$, $\dot{\eta}_i(0) = 0$. The amplitudes of the oscillations decay in the former case, whereas it grows and saturates in the latter case. This indicates that non-normality of the system leads to transient growth that triggers nonlinearities, in the presence of damping as well.

As shown in figure 7(*c*), the phase evolves to 90° indicating the absence of acoustic driving for the first case. However, as damping is present, the oscillations decay.

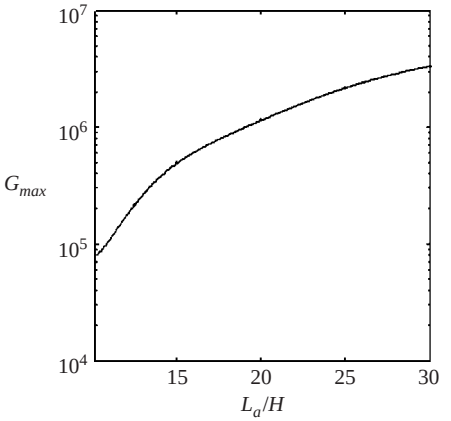

FIGURE 8. The variation of maximum growth factor with duct length to duct width ratio. The flame is located at 1/4 duct length, $Pe = 10$, $X_i = 3.2/7$, $Y_i = 3.2$, $\alpha = 0.25$.

Figure 7(*d*) shows that the phase difference is not 90° as the amplitudes saturate in the second case. As we approach the limit cycle, the phase difference tends to a value which will result in just adequate driving to balance the damping in the system. Though damping is not essential for saturation to occur, it plays an important role in the evolution of the perturbation.

7.4. *Transient growth*

In this section, the dependence of the transient growth factor on various parameters such as Péclet number, slot width, and the ratio of combustion scale to acoustic length scale is studied. The effect of damping is not taken into account, as it is highly system specific. First, the variation of growth factor with duct length to duct width ratio is studied. This ratio is found to be critical in combustion instability (Tyagi *et al.* 2007). Figure 8 shows the variation of the maximum growth factor with duct length to duct width ratio for a flame that is located at 1/4 duct. The non-dimensional slot width is chosen as 0.25, $Pe = 10$ and $X_i = 3.2/7$, $Y_i = 3.2$. It is observed that the growth factor increases monotonically. This implies that the growth factor becomes larger as the flame becomes more compact. The heat release rate is considered to be a point source in our analysis. The strength of this point source increases as the flame becomes more and more compact, causing the flame to be a stronger source for the acoustics. Hence, the growth factor is larger for a compact flame.

Figure 9 shows the variation of growth factor with Péclet number for a flame located at 1/4 duct length. The non-dimensional fuel slot width is 0.25, $X_i = 3.2/7$, $Y_i = 3.2$ and $L_a/2H = 12.50$. It is clear that the growth factor increases monotonically. This is because non-normality becomes pronounced as the convective effects become significant, i.e. large Péclet numbers. The growth factor is infinite for Péclet numbers larger than 25, indicating that the thermoacoustic oscillations are linearly unstable.

Figure 10 shows the variation of growth factor with slot-width ratio for a flame located at 1/4 duct length. The Péclet number is 10.0, $X_i = 3.2/7$, $Y_i = 3.2$ and $L_a/2H = 12.50$. The growth factor is infinite for $\alpha \leqslant 0.1$, which indicates that the system is linearly unstable for $\alpha \leqslant 0.1$. It is seen that the variation of growth factor with slot width is non-monotonic.

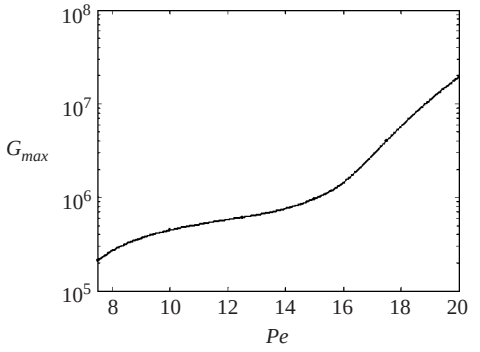

FIGURE 9. The variation of maximum growth factor with Péclet number. The flame is located at 1/4 duct length, $\alpha = 0.25$, $X_i = 3.2/7$, $Y_i = 3.2$, $L_a/2H = 12.5$.

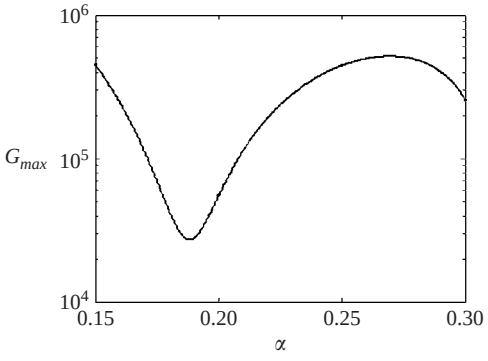

FIGURE 10. The variation of maximum growth factor with fuel slot width to duct width ratio. The flame is located at 1/4 duct length, and $Pe = 10$, $X_i = 3.2/7$, $Y_i = 3.2$, $L_a/2H = 12.5$.

7.5. *Pseudospectra*

As discussed in § 5, the non-normal nature of an operator can be studied using the geometry of the pseudospectra. Necessary and sufficient conditions for a system not to exhibit growth (transient or exponential) are obtained based on the geometry of the pseudospectra. Trefetehen *et al.* (1993) have used the relation between geometry of the pseudospectra and the lower bound on the transient growth factor to analyse hydrodynamic instability in Couette and Poiseuille flows. The lower bound on the transient growth factor is given by

$$\max_t \|e^{tA}\| \geqslant \max_\varepsilon \frac{\max_{z\in\Gamma(\varepsilon)} Re(z)}{\varepsilon}. \tag{27}$$

It is clear from (27) that if the contour protrudes far into the right-hand half-plane, then the system will exhibit large transient growth. Hence, for a system not to grow (transient for any initial condition or exponential growth), pseudospectra must lie entirely on the left half-plane. This is a necessary condition.

Further, the relation between the upper bound on the transient growth factor and the geometry of pseudospectra is used to obtain a sufficiency condition for a system to be stable. The evolution operator e^{tA} can be defined by the Dunford–Taylor integral

(operator analogue of the Cauchy integral),

$$e^{tA} = \frac{1}{2\pi i}\int_{\Gamma}(z-A)^{-1}e^{tz}dz, \tag{28}$$

where $\Gamma(\varepsilon)$ is the boundary of pseudospectra corresponding to some ε. Hence, the norm of the evolution operator is bounded by the Cauchy integral of $|e^{tz}|\|(z-A)^{-1}\|$. When Γ encloses the ε-pseudospectra, then the upper bound for the transient growth factor can be written as (Trefethen & Embree 2005),

$$\|\exp(tA)\| \leqslant \left[\frac{L_\varepsilon}{2\pi\varepsilon}\max_{z\in\Gamma(\varepsilon)}|\exp(tz)|\right]. \tag{29}$$

where L_ε is the length of the contour (or convux hull) $\Gamma(\varepsilon)$. Choosing A as the stability operator L, the upper bound on the maximum growth rate is given by,

$$G_{max} = \max_t \|\exp(tL)\|^2 \leqslant \max_t \left[\frac{L_\varepsilon}{2\pi\varepsilon}\max_{z\in\Gamma(\varepsilon)}|\exp(tz)|\right]^2. \tag{30}$$

Hence a system is stable if the real parts of all the eigenvalues are negative and if the right-hand side of the above expression is 1. Hence, if the pseudospectra lies entirely in the left-hand half-plane and if $G_{max} = 1$, then the system will not grow for any initial condition.

The Rayleigh criterion gives the condition for acoustic driving to occur. However, the prediction of transient growth by Rayleigh criteria requires precise knowledge of the initial conditions. The ambiguity of initial conditions owing to noise makes the identification of transient growth using Rayleigh criteria difficult. However, the necessary and sufficiency conditions obtained in this paper are conditions on the operator and hence do not depend on the initial conditions.

Figure 11 shows the pseudospectra for a thermoacoustic system with $Pe = 10$, $X_i = 3.2/7$, $Y_i = 3.2$, $L_a/2H = 12.5$. As in § 7.4, the effect of damping is not taken into account, as it is highly system specific. It is clear from the non-circular behaviour that the system is highly non-normal. Figure 11(*a*) shows the nature of pseudopsectra close to the origin. It is clear that the contour is not entirely on the left half-plane. Hence, it can be inferred from (27) that this system shows transient growth. This indicates that there is an 'unstable' pseudoeigenvalue for some ε. Even if a system behaves linearly, the transient growth can cause the amplitudes to reach high values, which could lead to triggering. Figure 11(*b*) shows the pseudospectra over a larger domain. It can be seen from figure 11(*b*) that the pseudospectra taper towards the left-hand half-plane. This indicates that eigenvalues with large negative real part are less sensitive to perturbations. This could be helpful in identifying the significance of a particular mode in thermoacoustic oscillations.

8. Discussion

Current linear-system-identification approaches in the time domain, such as the impulse response of the flame, give the combustion response in the time domain (Polifke 2004), which indeed has the information on non-normality. However, current network models convert the system response in time domain to a flame transfer function in the frequency domain, and neglect the non-orthogonality of the eigenvectors. This results in their failure to predict transient growth. However, the current linear-system identification tools in the time domain, along with the tools

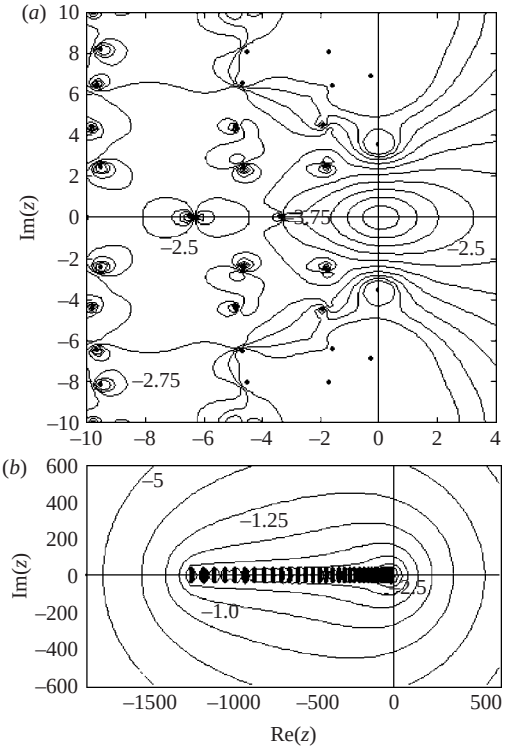

FIGURE 11. (*a*) The pseudospectra of the thermo-acoustic system near the origin, (*b*) pseudospectra about all the eigenvalues. The flame is located at 1/4 duct length, and $Pe = 10$, $L_a/2H = 12.5$, $X_i = 3.2/7$, $Y_i = 3.2$, $\alpha = 0.25$. The dots denote the eigenvalues. The value of $\log_{10} \varepsilon$ is indicated next to the contours.

based on the linearized operator suggested in this paper can indeed be used to predict transient growth.

9. Conclusion

In this paper, the nature of flame acoustic interaction is studied in the context of diffusion flames. The coupled combustion–acoustic system is non-normal and hence the eigenvectors are non-orthogonal. Non-normality leads to short-time amplification even though the individual modes decay exponentially. This transient growth can trigger nonlinearities when the amplitude of the fluctuations is sufficiently large. It has been observed that the various eigenmodes of the coupled combustion–acoustic system interact resulting in the growth of oscillations, even when the eigenvalues indicate stability. Non-normality and nonlinearity lead to triggering and redistribution of energy between eigenmodes. Further, saturation occurs irrespective of the presence or absence of damping. In the absence of damping, as the system approaches the limit cycle, the phase difference between the pressure fluctuations and heat release rate oscillations approaches 90°. In the presence of damping, the phase difference approaches a value which will result in adequate driving to balance the damping.

An analysis of transient growth revealed that the growth factor increased monotonically with the ratio of the acoustic to combustion length scale and Péclet number. However, the variation of growth factor with the non-dimensional slot width

was not monotonic. For a non-normal system, 'pseudoresonance' is shown to occur at frequencies far from the spectrum. The stability and sensitivity of non-normal systems can be studied using pseudospectra. The pseudospectra of normal operators are disjoint circles. The pseudospectra of the thermoacoustic system are non-circular, implying a highly non-normal nature of the system. If the pseudospectra are not entirely within the left half-plane, then the system can show transient growth. It is possible to identify systems which cannot show transient growth by analysing the pseudospectra. The geometry of the pseudospectra provides necessary and sufficient conditions for the stability of a system.

The current methodology for studying the onset of thermoacoustic oscillations involves looking for exponentially growing or decaying modes by calculating the individual eigenvalues of the linearized system. Further, the nonlinear behaviour of the combustion response is modelled using flame transfer functions which are amplitude dependent. These approaches fail to predict phenomena such as nonlinear growth triggered by the transient growth which results from the non-normality of the thermoacoustic system and excitation of frequencies that are not initially excited. More sophisticated approaches have to be taken and more involved methods have to be introduced, to capture accurately the transient behaviour which is critical for the overall system stability. However, the current linear system identification tools in the time domain, along with the tools based on the linearized operator suggested in this paper such as growth factor and pseudospectra, can be used to predict transient growth.

This work was funded by the Department of Science and Technology. The authors wish to thank Professor Wolfgang Polifke (Technishe Universität München, Germany) for his critical comments and suggestions. We also thank Dr Nandan Sinha (IIT Madras) Srevatsan Muralidharan (IIT Madras, currently at Princeton University) and Professor Rama Govindarajan (Jawaharlal Nehru Centre for Advanced Scientific Research, Bangalore) and Dr V. Sidddartha (retired scientist, DRDO) for their suggestions and interesting discussions.

Appendix A

It is shown in the following that in the infinite-rate chemistry assumption, the pressure fluctuation term in the energy equation can be neglected

$$\rho C_p \frac{\partial T}{\partial t} + \rho C_p u \frac{\partial T}{\partial x} = \kappa \nabla^2 T + \frac{\mathrm{d}p'}{\mathrm{d}t}.$$

The above equation is non-dimensionalized as follows:

$$\frac{\rho C_p T_{st}}{t_{comb}} \frac{\partial T^*}{\partial t^*} + \frac{\rho C_p u T_{st}}{\bar{u} t_{comb}} \frac{\partial T^*}{\partial x^*} = \frac{\kappa \rho C_p T_{st}}{\kappa t_{comb} Pe} \nabla^2 T^* + \frac{\rho R T_{st}}{t_{ac}} \left(\frac{\mathrm{d}p'^*}{\mathrm{d}t^*} \right)_{acoustic}.$$

The changes within the combustion zone happens at combustion time scales (t_{comb}) except the pressure fluctuation which happens at acoustic time scale (t_{ac}). The above equation simplifies to

$$\frac{\partial T^*}{\partial t^*} + u^* \frac{\partial T^*}{\partial x^*} = \frac{1}{Pe} \nabla^2 T^* + \frac{t_{comb}}{t_{ac}} \left(\frac{\mathrm{d}p'^*}{\mathrm{d}t^*} \right)_{acoustic}.$$

Hence, in the infinite-rate chemistry assumption ($t_{comb}/t_{ac} \to 0$), the last term on the right-hand hand side can be neglected. Hence, the non-dimensionalized energy

equation can be written as

$$\frac{\partial T^*}{\partial t^*} + u^* \frac{\partial T^*}{\partial x^*} = \frac{1}{Pe} \nabla^2 T^*.$$

Appendix B

The steady Burke–Schumann solution is given by

$$Z_{st} = X_i(1-\alpha) - Y_i\alpha + \sum_n \frac{\cosh m_n(x-L)}{\cosh m_n L} \cos(n\pi y) - \frac{2[(X_i + Y_i)\sin(n\pi\alpha)]}{n\pi},$$

where

$$m_n = Pe/2 - \sqrt{Pe^2/4 + n^2\pi^2}.$$

The expanded forms of the matrices used in (22) are presented below.

$$\chi = \left[G_1^1\ G_2^1 \cdots G_m^n \cdots G_M^N\ \eta_1\ \eta_2 \cdots \eta_K\ \dot{\eta}_1/\pi\ \dot{\eta}_2/2\pi \cdots \dot{\eta}_K/K\pi\right]^T M = I + \frac{2}{(T_i + T_{ad})/2} M_1,$$

where, matrix M_1 can be written as a column vector and a row vector as follows,

$$M_1 = \begin{bmatrix} 0 \\ . \\ 0 \\ 0 \\ . \\ 0 \\ \sin \pi x_f \\ \sin 2\pi x_f \\ . \\ \sin K\pi x_f \end{bmatrix} [R_{11}\ R_{12} \ldots R_{NM\times NM}\ 0\ 0 \ldots 0]_{(NM+2K)\times(NM+2K)}$$

The non-normal matrix can be expanded as $B_{NN} = -D + A_1 - A_2 + A_3 - A_4$.
The nonlinear matrix can be expressed as $B_{NL} = A_1[u(t)-1]$.

$$D = \begin{bmatrix} D_1^1 & & & & & & & & \\ & D_2^1 & & & & & & & \\ & & . & & & & & & \\ & & & D_m^n & & & & & \\ & & & & . & & & & \\ & & & & & . & & & \\ & & & & & & D_M^N & & \\ & & & & & & & 0 & \\ & & & & & & & & . \\ & & & & & & & & & 0 \end{bmatrix},$$

where $D_m^n = -[(m+1/2)^2\pi^2/L^2 + n^2\pi^2]/Pe$.

$$A_1 = \begin{bmatrix} [W^{(1)}] & & & & & & & \\ & [W^{(2)}] & & & & & & \\ & & . & & & & & \\ & & & . & & & & \\ & & & & [W^{(NM)}] & & & \\ & & & & & 0 & & \\ & & & & & & 0 & \\ & & & & & & & . \\ & & & & & & & & . \\ & & & & & & & & & 0 \end{bmatrix}, \quad [W^{(i)}] = \begin{bmatrix} W_{11} & W_{12} & . & . & W_{1M} \\ W_{21} & W_{22} & . & . & W_{2M} \\ . & . & . & . & . \\ . & . & . & . & . \\ W_{M1} & W_{M2} & . & . & W_{MM} \end{bmatrix}.$$

Matrix A_2 can be written as a product of a column vector and row vector as follows:

$$A_2 = -\begin{bmatrix} 0 \\ . \\ 0 \\ \cos(\pi x_f) \\ . \\ \cos(K\pi x_f) \\ 0 \\ . \\ 0 \end{bmatrix} \begin{bmatrix} C_1^{(1)} C_2^{(1)} \dots C_{NM}^{NM} \, 0 \, 0 \dots 0 \end{bmatrix}_{(NM+2K)\times(NM+2K)}.$$

Matrix A_3 is given by, $A_3 = \begin{bmatrix} [0]_{NM\times NM} & [0]_{NM\times 2K} \\ [0]_{2K\times NM} & [S]_{2K\times 2K} \end{bmatrix}$,

where $S = \begin{bmatrix} 0 & 0 & . & 0 & -\pi & 0 & 0 & 0 \\ 0 & 0 & . & 0 & 0 & -2\pi & 0 & 0 \\ . & . & . & . & . & . & . & . \\ 0 & 0 & 0 & 0 & 0 & 0 & 0 & -K\pi \\ \pi & 0 & 0 & 0 & -2\xi_1 & 0 & 0 & 0 \\ 0 & 2\pi & 0 & 0 & 0 & -2\xi_2 & 0 & 0 \\ . & . & . & . & . & . & . & . \\ 0 & 0 & 0 & K\pi & 0 & 0 & 0 & -2\xi_K \end{bmatrix}$,

$$A_4 = -\frac{2}{(T_i + T_{ad})/2} Q_{st} F_1,$$

$$F_1 = \begin{bmatrix} 0 \\ 0 \\ . \\ . \\ 0 \\ 0 \\ . \\ 0 \\ \sin \pi x_f \\ \sin 2\pi x_f \\ . \\ \sin K\pi x_f \end{bmatrix} \begin{bmatrix} 0 \, 0 \dots 0 \, \cos \pi x_f \, \cos 2\pi x_f \dots \cos K\pi x_f \, 0 \, 0 \dots 0 \end{bmatrix}_{(NM+2K)\times(NM+2K)}.$$

REFERENCES

Ananthkrishnan, N., Deo, S. & Culick, F. E. C. 2005 Reduced-order modeling and dynamics of nonlinear acoustic waves in a combustion chamber. *Combust. Sci. Tech.* **177**, 221–247.

Baggett, J. S., Driscoll, T. A. & Trefethen, L. N. 1995 A mostly linear model of transition to turbulence. *Phys. Fluids* **7**, 833–838.

Balasubramanian, K. & Sujith, R. I. 2007 Thermoacoustic instability in a Rijke tube: non-normality and nonlinearity, AIAA 2007-3428, *13th AIAA/CEAS Aeroacoustics Conf. Rome, Italy, May 21–23.*

Buckmaster, J. 2002 Edge-flames. *Prog. Energy Combust. Sci.* **28**, 435–475.

Buckmaster, J., Jackson, T. L. & Yao, J. 1999 An elementary discussion of propellant flame geometry. *Combust. Flame* **117**, 541–552.

Chaos, M., Chen, R. H., Welle, E. J. & Roberts, W. L. 2005 Fuel Lewis number effects in unsteady Burke–Schumann hydrogen flames. *Combust. Sci. Technol.* **177**, 75–88.

Chung, S. H. & Law, C. K. 1984 Burke–Schumann flame with streamwise and preferential diffusion. *Combust. Sci. Technol.* **37**, 21–46.

Culick, F. E. C., Burnley, V. & Swenson, G. 1995 Pulsed instabilities in solid propellant rockets. *J. Propul. Power* **11**, 657–665.

Cuenot, B., Egolfopoulos, F. N. & Poinsot, T. 2000 An unsteady laminar flamelet model for non-premixed combustion. *Combust. Theory Modelling* **4**, 77–97.

Dowling, A. P. 1995 The calculation of thermoacoustic oscillations. *J. Sound Vib.* **180**, 557–581.

Dowling, A. P. & Stow, S. R. 2003 Acoustic analysis of gas turbine combustors. *J. Propul. Power* **19**, 751–764.

Farrell, B. F. 1989 Optimal excitation of baroclinic waves. *J. Atmos. Sci.* **46**, 1193–1206.

Fichera, A., Losseno, C. & Pagano, A. 2001 Clustering of chaotic dynamics of a lean gasturbine combustor. *Appl. Energy* **69**, 101–117.

Gebgart, T. & Grossmann, S. 1994 Chaos transition despite linear stability. *Phys. Rev.* E **50**, 3705–3711.

Handel, A. 2004 Limits of localized control in extended nonlinear systems. PhD thesis School of Physics, Georgia Institute of Technology.

Heckl, M. A. 1990 Nonlinear acoustic effects in a Rijke tube. *Acustica* **72**, 63–71.

Henningson, D. S. & Schmid, P. J. 1992 Vector eigen function-expansion for plane channel flows. *stud. Appl. Maths* **87**, 15–43.

Hertzberg, J. R. 1997 Conditions for a Split Diffusion Flame. *Combust. Flame* **109**, 314–322.

Jackson, T. L. & Buckmaster, J. 2000 Nonpremixed periodic flames supported by heterogeneous propellants. *J. Propul. Power* **16**, 498–504.

Kerner, W. 1989 Large scale complex eigenvalue problems. *J. Comput. Phys.* **85**, 1–85.

Kurdyumov, V. N. & Matalon, M. 2004 Dynamics of an edge flame in a mixing layer. *Combust. Flame* **139**, 329–339.

Lang, W. 1991 Harmonic frequency generation by oscillating flames. *Combust. Flame* **83**, 253–262.

Lieuwen, T. 2003 Modeling premixed combustion acoustic wave interactions: a review. *J. Propul. Power* **19**, 765–781.

Matveev, K. I. 2003 Thermo-acoustic instabilities in the Rijke tube: experiments and modeling. PhD thesis, California Institute of Technology.

Matveev, K. I. & Culick, F. E. C. 2003 A model for combustion instability involving vortex shedding. *Combust. Sci. Technol.* **175**, 1059–1083.

Mcmanus, K., Poinsot, T. & Candel, S. M. 1993 A review of active control of combustion instabilities. *Prog. Energy Combust. Sci.* **19**, 1–29.

Meirovitch, L. 1967 *Analytical Methods in Vibrations.* Macmillan.

Polifke, W. 2004 Numerical techniques for identification of acoustic multi-ports. In *Advances in Aeroacoustics and Applications*, VKI Lecture Series Monographs 2004–05. Von Karman Institute, Brussels.

Reddy, S. C. & Trefethen, L. N. 1994 Pseudospectra of the convection–diffusion operator. *SIAM J. Appl. Maths* **54**, 1634–1639.

Schadow, K., Gutmark, E., Parr, T., Parr, K., Wilson, K. & Crump, J. 1989 Large-scale coherent structures as drivers of combustion instability. *Combust. Sci. Technol.* **64**, 167–186.

Schmid, P. J. & Henningson, D. S. 2001 *Stability and Transition in Shear Flows.* Springer.

Trefethen, L. N. 1997 Pseudospectra of linear operators. *SIAM Rev.* **39**, 383–406.

Trefethen, L. N. & Embree, M. 2005 *Spectra and Pseudospectra*. Princeton University Press.

Trefethen, L. N., Trefethen, A. E., Reddy, S. C. & Driscoll, T. A. 1993 Hydrodynamic stability without eigenvalues. *Science* **261**, 578–584.

Tyagi, M., Chakravarthy, S. R. & Sujith, R. I. 2007 Unsteady response of a ducted non-premixed flame and acoustic coupling. *Combust. Theory Modeling* **11**, 205–226.

Vance, R., Miklavcic, R. & Wichman, I. S. 2001 On the stability of one-dimensional diffusion flames established between plane, parallel, porous walls. *Combust. Theory Modeling* **5**, 2001, 147–161.

Wicker, J. M., Greene, W. D., Kim, S.-I. & Yang, V. 1996 Triggering of longitudinal combustion instabilities in rocket motors: nonlinear combustion response. *J. Propul. Power* **12**, 1148–1158.

Wu, X.,Wang, M., Moin, P. & Peters, N. 2003 Combustion instability due the nonlinear interaction between sound and flame. *J. Fluid Mech.* **497**, 23–53.

Yoon, H. G., Peddieson, J. & Purdy, K. R. 2001 Nonlinear response of a generalized Rijke tube. *Intl. J. Engng. Sci.* **39**, 1707–1723.

Zinn, B. T. & Lieuwen, T. C. 2005 Combustion instabilities: basic concepts. *Combustion Instabilities in Gas Turbine Engines: Operational Experience, Fundamental Mechanisms, and Modeling* (ed. T. C. Lieuwen & V. Yang), chap. 1. *Progress in Astronautics and Aeronautics*, vol. 210. AIAA.